Liquid-crystalline poly(azomethine)s: 1. Thermodynamic properties

Stephen Z. D. Cheng, James J. Janimak, Krishnamurthy Sridhar and Frank W. Harris

Institute and Department of Polymer Science, The University of Akron, Akron, Ohio 44325, USA

(Received 13 May 1988; revised 5 July 1988; accepted 8 July 1988)

A new series of liquid-crystalline poly(azomethine)s (PAMEs), containing different numbers n of ethylene glycol flexible spacers, has been studied. It has been observed that, after crystal melting, all specimens show nematic liquid-crystalline phases before they reach their isotropic melts. The polymers can form single liquid-crystalline glassy phases after quenching ($n=1$) or on cooling ($n=2$, 3 and 4). The heat capacities of the polymers in solids, nematic liquid crystals and isotropic melts have been measured in the temperature range 230–620 K. Calculations of the solid heat capacities of the polymers have been carried out based on their vibrational spectra. The liquid-crystalline glass transitions of the polymers have been investigated. Pre-glass transitions of the PAMEs have been distinguished in lower-temperature regions, and they are attributed to the contributions of flexible spacers. Broadness of the semicrystalline PAMEs in the glass transition regions is reported. Hysteresis effects of PAMEs show a dependence on the number of flexible spacers. Both transitions from rigid crystals to nematic liquid crystals and from nematic liquid crystals to isotropic melts were studied. The enthalpy and entropy changes are discussed systematically.

(Keywords: crystal; enthalpy; entropy; glass transition; heat capacity; hysteresis; liquid-crystalline glass; liquid crystal; mesophase; nematic; poly(azomethine); thermodynamic properties)

INTRODUCTION

The discovery of poly(azomethine)s (PAMEs) can be traced back about 60 years. The first PAME sample was prepared by Adams and coworkers[1] from terephthalaldehyde, benzidine and dianisidine. During the 1950s, Marvel and coworkers prepared a number of polyazines and PAMEs from aromatic dialdehydes with hydrazine and *o*-phenylenediamine, and examined their chelate formation and thermal stability[2–4]. Cotter and Matzner[5] summarized this development in 1967, and D'Alelio[6] has reviewed this progress in 1969, based primarily on his own work. Recently, Morgan and coworkers have reported the preparation of a variety of wholly aromatic melt anisotropic PAMEs and their fibres[7–9]. Their polymers showed high melting temperatures and potential usage in engineering applications. Furthermore, the melting temperature can also be controlled by ring substitution, copolymerization and/or the introduction of limited chain flexibility. The dilute-solution properties of some PAMEs have also been investigated by Milland *et al.*[10–12]. From the viscosity law and the variation of the apparent molecular anisotropy, the rigidity of the molecule has been evaluated. The persistence length has been found to be about 15 nm.

The introduction of flexible spacers into the main chains of aromatic PAMEs has been studied very recently[13] by systematic variations in the numbers of both mesogenic groups and flexible spacers. Three series of melt-spinnable thermotropic poly(azomethine ether)s have been synthesized with different lengths of flexible spacers.

Various characterizations, such as both transition temperatures (isotropic melting and anisotropic melting), mechanical tests, X-ray analyses and density measurements, have been reported mainly for fibre-made polymers.

In this paper, as the first paper in this series, we will report detailed thermodynamic properties for a new series of PAMEs containing different numbers n of flexible spacers (ethylene glycol; $n=1$, 2, 3 and 4). They were synthesized at The University of Akron[14]. All samples show nematic liquid-crystalline phases before they reach their isotropic melts. An interesting feature is that the samples can be quenched ($n=1$) or cooled ($n=2$, 3 and 4) to below their glass transition temperatures, to produce a single nematic glassy phase (liquid-crystalline or LC glass)[15] from their nematic liquid-crystalline states. This permits the study of LC glass transition behaviour, and comparison with normal amorphous glass transition behaviour based on our heat capacity measurements in the four states (semicrystalline, LC glass, nematic liquid crystal and isotropic melt). Calculation of the heat capacities in their solid states has been performed based on independent infra-red and Raman measurements, as well as on vibrational dispersion curves established by normal-mode calculations for the polymers. The equilibrium thermodynamic properties, such as the changes of enthalpy and entropy of both transitions, namely the transitions from rigid crystal to nematic liquid-crystalline phase (disordered transitions) and the transitions from nematic liquid crystal to isotropic melt (isotropic transitions), are studied. The number of flexible spacers has been correlated not only with disordered and isotropic transition temperatures but also with their enthalpy and entropy changes. A systematic analysis for

0032-3861/89/030494-10$03.00

the thermodynamic properties of these new PAMEs is addressed. It seems that the mesophase transitions observed have provided a set of new examples which can be fitted well into our general discussion of the nematic liquid-crystalline transition. It is well known that, for a typical nematic liquid-crystal transition in macromolecules, the entropy change is only about 2–5% of the total entropy change from rigid crystal to isotropic melt[15].

MATERIALS AND EXPERIMENTS

This new series of poly(azomethine)s was synthesized in our laboratory at The University of Akron. Synthesis procedures involve both monomer synthesis and polymerization steps. They have been described in detail in refs. 14 and 16. The chemical structures of the repeat units and their molecular masses are as follows:

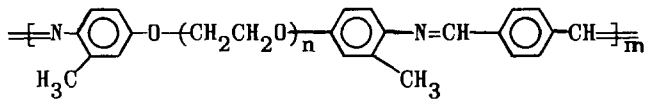

$n=1$ $MW=370.5\,\mathrm{g\,mol^{-1}}$

$n=2$ $MW=414.6\,\mathrm{g\,mol^{-1}}$

$n=3$ $MW=458.6\,\mathrm{g\,mol^{-1}}$

$n=4$ $MW=502.7\,\mathrm{g\,mol^{-1}}$

The inherent viscosities of these four PAMEs in methane sulphonic acid at 303 K were 0.47, 0.69, 0.66 and 0.91 $\mathrm{dl\,g^{-1}}$, respectively. The PAME samples for differential scanning calorimetry (d.s.c.) were enclosed in aluminium pans. The sample weights were over 15 mg in order to obtain sufficient sensitivity for heat capacity measurements. The precision of the sample weight was ± 0.001 mg. The weights of the empty pan, reference pan and sample pan were controlled to within ± 0.001 mg. The samples for wide-angle X-ray scattering (WAXS) were prepared in a ground powder dispersion. The powder can also be pressed thermally into films between two glass slides with about a 0.01 mm separation thickness. Their phase transition behaviour can thus be studied under an AO polarizing optical microscope.

The samples were measured with an updated computer-interfaced Perkin–Elmer DSC2 in our laboratory. The DSC2's analog output is now converted to a digital interface and then fed into an IBM personal computer for data handling. The software was developed and installed by Laboratory Microsystems Inc.

The heat capacity runs were performed in three selected temperature ranges: from 220 K to below their glass transition temperatures T_g, for the solid heat capacity measurements; from T_g to above the isotropic transition temperature T_i, for analysis of the two-phase transition regions; and in the temperature region above T_i to below their decomposition temperature, for measurements of the heat capacity in the liquid state (except for $n=1$ where T_i is higher than its decomposition temperature). The DSC2 was calibrated in these three temperature regions following standard procedures[17]. Both temperature and heat-flow scales were corrected by using standard materials. The reproducibility of our Al_2O_3 heat capacity calibration was within $\pm 0.01\%$ based on data of the National Bureau of Standards[18]. Both the heating and cooling rates were kept at 10 K $\mathrm{min^{-1}}$. In order to detect the hysteresis effect, different cooling rates (-0.31 to $-10\,\mathrm{K\,min^{-1}}$) were used with indication. The glass transition regions were characterized by five temperatures, as before[19]. The first perceptible beginning of the glass transition, T_b, is judged by the initial increase in heat capacity from that of the solid state (glassy or crystalline). The extrapolated beginning and end of the glass transition are expressed by T_1 and T_2 and are indicative of the broadness of the major portion of the glass transition. The glass transition temperature T_g is chosen at half-devitrification when judged by the increase in heat capacity. Finally, T_e, the end of glass transition, is reached when the heat capacity matches the liquid heat capacity. In case of hysteresis at the glass transition, the peak temperature and the heat of the hysteresis peak are also recorded (as the integration of C_p above the liquid baseline with respect to temperature).

An AO interference optical microscope was used with a Mettler FP2 hot stage. It is fundamentally a polarizing microscope modified into a two-beam interferometer[20]. The condenser has a birefringent plate which divides the incoming light into two beams, and the objective has a corresponding plate which recombines the two split beams after one has passed through the specimen (NA 0.25, 40× magnification). Above the objective is a quarter-wave compensator as an analyser. The eyepiece used was a double-focus type 20× objective, so that visual observations were made at 800× magnification. The polarizer underneath the condenser polarizes the light in a plane at 45° to the axis of the birefringent plate. Photographs were taken with a 35 mm camera so that typically the long edge of the figures represents 0.012 mm. The temperature scale of the hot stage was also calibrated by using standard materials.

WAXS experiments were carried out on a Rigaku X-ray generator with a 12 kW rotating anode as a source of the incident X-ray beam. The line-focused beam is monochromatized with a graphite crystal and a pulse-height analyser to Cu K_α radiation. A D/Max-B X-ray powder diffractometer was controlled by an IBM personal computer. The range of scanning angle (2θ) was 0–50° to determine the crystallinities of the samples. A temperature controller was added on to the X-ray apparatus for thermal measurements. The precision of the controller was ± 0.1 K in the temperature range between room temperature and 620 K. Programmed heating and cooling can also be performed under control. The samples were scanned at different temperatures at which different states appeared based on d.s.c. measurements (see below). X-ray diffraction photographs are taken using a point-focused beam. The temperature controller on the X-ray apparatus was also calibrated.

RESULTS

Optical properties of the mesophases in PAMEs

At room temperature all four polymer samples show strong birefringences which are characterized as rigid crystalline phases. Using the hot stage (Mettler FP2) to heat the samples at 10 K $\mathrm{min^{-1}}$, one can see a drastic change of birefringence patterns at a temperature of 538 K for PAME ($n=1$), 440 K for PAME ($n=2$), 417 K

for PAME ($n=3$) and 369 K for PAME ($n=4$). Above those temperatures, flowed schlieren textures with thread-like lines can be seen, as shown in *Figure 1a*, as an example of PAME ($n=4$). Continuous heating leads to a change of birefringence again to zero extinction at 568 K for PAME ($n=2$), 513 K for PAME ($n=3$) and 468 K for PAME ($n=4$). The PAME ($n=1$) sample does not show any birefringence change up to the temperature limit of our hot stage (573 K). Interestingly enough, during cooling to room temperature, one can find that for PAMEs ($n=2$, 3 and 4) the birefringence patterns change back to the schlieren textures again at the same temperatures as indicated previously (higher temperatures). Nevertheless, there is no further birefringence change back to the rigid crystalline phases at lower temperatures. The schlieren textures are still present on cooling the samples to room temperature, as shown in *Figure 1b*, which was taken at 298 K for PAME ($n=4$). In the case of PAME ($n=1$) the second change of birefringence to its rigid crystalline phase is observed during cooling at about 445 K, lower than the change in temperature observed on heating (538 K).

X-ray diffraction experiments of PAMEs

Even though it is our purpose to study the crystalline structures and morphology of the PAMEs, we only report our X-ray diffraction results of the crystallinity determination here and keep our further results to be published in the second paper of this series[21].

Figure 2a shows an X-ray photograph of PAME ($n=3$), as an example. At least eight diffraction rings are observed, and their corresponding angles are shown in *Figure 2c*. Increasing the temperature to above their disordered transition temperature T_d, however, one can find that only one strong diffuse ring at $2\theta=21.4°$ is observed, as shown in *Figure 2b*. *Figure 2c* represents the relationship between intensity of the diffraction and angle 2θ for the semicrystalline, the mesophase and the isotropic melt states of PAME ($n=3$). One can find that the X-ray results from both mesophase and isotropic melt are substantially the same. Since the ratio of the scattering intensities due to the crystalline and amorphous regions is nearly equal to the ratio of the masses of the two types of region, we can determine the crystallinity, which is defined in terms of its total mass and the respective masses of the crystalline and amorphous components.

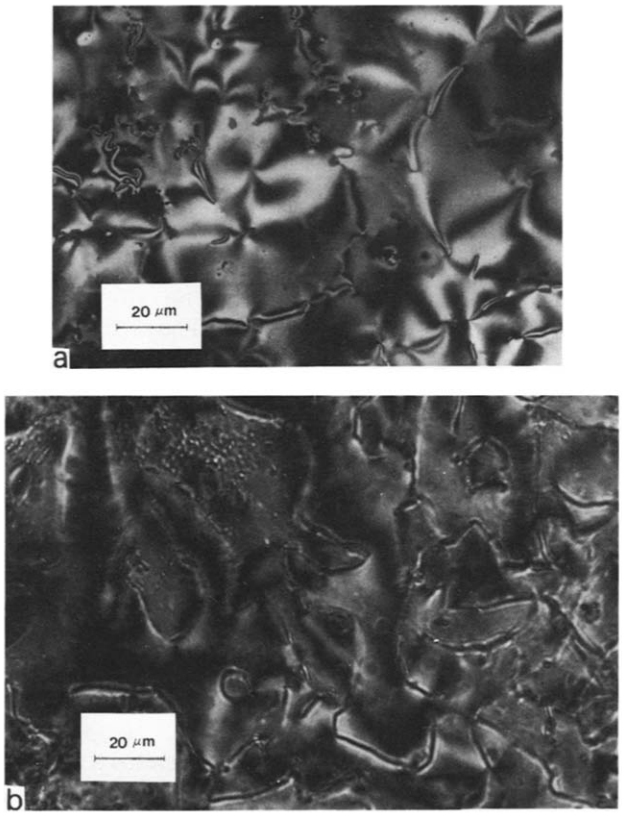

Figure 1 (a) Flowed schlieren texture of PAME ($n=4$) at 462.5 K under polarized optical microscope. (b) A similar texture of PAME ($n=4$) can be observed at 298.2 K under polarized optical microscope

Our measurements indicate that for the PAMEs as polymerized (semicrystalline samples), their crystallinities are 50.0%, 26.9%, 38.5% and 19.1% (*Table 1*) for the PAMEs ($n=1$, 2, 3 and 4), respectively. Surprisingly, one can find that both PAMEs with an odd number of flexible spacers, i.e. $n=1$ and $n=3$, have relatively high crystallinities. The other two PAMEs with an even number of flexible spacers, i.e. $n=2$ and $n=4$, on the other hand, have lower crystallinities. From our X-ray diffraction patterns, it is clear that the crystalline structure of odd numbers of flexible spacers is different from that of even-numbered ones, and the results will be reported in the second paper of this series[21].

Solid-state heat capacities of PAMEs

The experimental temperature range for the heat capacity measurements of PAMEs starts at 230 K. Even though the main glass transitions occur above this temperature, only the solid heat capacity of PAME ($n=1$) can be determined, i.e. there is a temperature range (230–270 K) which is below the beginning temperature of glass transition, T_b. For PAME ($n=2$), such determination is very critical. Only over a very narrow temperature range (230–250 K) can measurements be made below its T_b. We cannot determine the solid heat capacities of PAMEs ($n=3$ and $n=4$) since their T_b values are below 230 K (see below).

Both semicrystalline samples (as polymerized) and mesophase glass samples of PAMEs ($n=1$ and $n=2$) are measured in the temperature ranges 230–270 K and 230–250 K, respectively, and agree to better than $\pm 1\%$ in these ranges. A tendency of lower heat capacity for semicrystalline PAMEs can be suggested, but is still in or at the border of experimental error. The solid-state heat capacities of PAMEs ($n=1$ and 2) were fitted to the following equations in $J\,K^{-1}\,mol^{-1}$ (root-mean-square deviations, $\pm 1.0\%$):

$$C_p = 0.000\,701\,78T^2 + 1.0658T + 70.174 \qquad (1)$$

for PAME ($n=1$), and

$$C_p = 0.001\,5529T^2 + 0.870\,83T + 120.76 \qquad (2)$$

for PAME ($n=2$).

Since we cannot determine the solid heat capacities of PAMEs ($n=3$ and $n=4$) experimentally, but because they are important to the study of transition behaviour, a theoretical calculation of the solid-state heat capacities for these four polymers is needed based on their vibrational spectra[22]. For chemically similar molecules, one can predict heat capacities even though their solid heat capacities have not been measured, as in the cases of PAMEs ($n=3$ and $n=4$) studied here.

The procedure of such calculations has been well

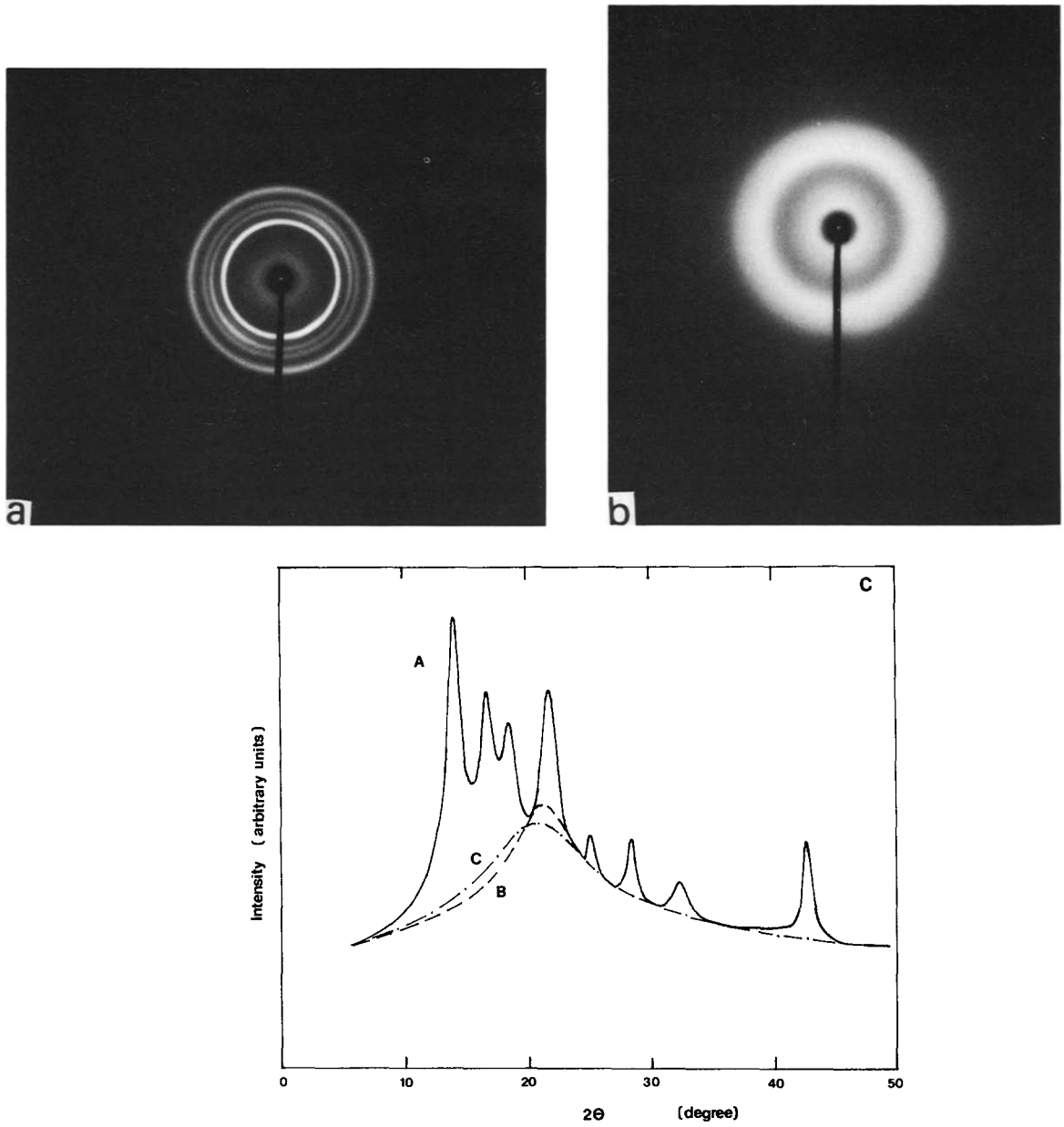

Figure 2 (a) X-ray diffraction pattern of semicrystalline PAME ($n=3$) as polymerized at 298.2 K. (b) X-ray diffraction pattern of PAME ($n=3$) at 480.2 K. (c) Relationship between X-ray intensity and 2θ for PAME ($n=3$) in the crystalline phase (A), the mesophase (B) and the isotropic melt (C)

Table 1 Thermal properties of PAMEs in the T_d and T_i transition regions measured on heating at 10 K min^{-1}

PAMEs	T_d (K)	ΔH_d (kJ mol^{-1})	ω_c [a] (%)	ΔH_d [b] (kJ mol^{-1})	ΔS_d [b] (J K^{-1} mol^{-1})	T_i (K)	ΔH_i (kJ mol^{-1})	ΔS_i (J K^{-1} mol^{-1})
$n=1$	534.7	20.2	50.0	40.4	75.5	?[c]	?[c]	?[c]
$n=2$	439.8	13.0	26.9	48.3	109.8	566.4	2.0	3.5
$n=3$	416.0	21.7	38.5	56.4	135.6	512.8	2.1	4.1
$n=4$	368.3	12.3	19.1	64.3	174.5	467.0	2.3	4.9

[a] The crystallinities quoted here were our X-ray data. From thermal measurements, one can also obtain the crystallinity under the assumption of two-phase model by $\omega_c = 1 - \Delta C_p(m)/\Delta C_p(a)$, where $\Delta C_p(m)$ and $\Delta C_p(a)$ are measured heat capacity increases at T_g for semicrystalline samples and 100% amorphous heat capacity increases. From this equation, the crystallinities are 59.9%, 32.1%, 43.9% and 23.2%. The differences between the two methods may be caused by 'rigid amorphous fractions' in the materials[19,29,30]

[b] Calculated for complete crystallization

[c] ?T_i for PAME ($n=1$) is higher than its decomposition temperature, and thus it cannot be determined

established[22-24]. The experimental heat capacities are taken in the case of PAME ($n=1$) and PAME ($n=2$) from our measurements (equations (1) and (2)). First, the contribution of the group vibrations to heat capacity is calculated and subtracted from the experimental value, constant-pressure heat capacity, C_p, after conversion to the constant-volume heat capacity, C_v. The remaining skeletal heat capacity is fitted to the Tarasov equation, $T(\theta_1/T, \theta_3/T)$, to obtain the limiting one- and three-dimensional vibrational frequencies, θ_1 and θ_3.

All frequencies in this discussion are, for convenience, expressed in kelvins ($1\,cm^{-1} = 1.4388\,K$). The detailed computer programs were given in a previous publication[25]. The C_p-to-C_v conversion is done using the Nernst–Lindemann equation since experimental data for the conversion are never available over the full temperature range:

$$C_p - C_v = C_p^2 A_0 T / T_m^\circ \quad (3)$$

where A_0, when expressed per mole of heavy atoms (C, O and N in this case), is often close to a universal constant[26] 5.11×10^{-3} K mol J^{-1} ($\pm 4 \times 10^{-3}$), and T_m° is the equilibrium melting temperature. The difference between C_p and C_v becomes larger than the experimental uncertainty in heat capacity only above about 200 K.

For the PAMEs, the skeletal vibrational modes are 25, 31, 37 and 43[22], and the group vibrational modes are 125, 140, 155 and 170 for $n = 1$, 2, 3 and 4, respectively. The group vibration spectra of (CH_2–CH_2–O), phenylene, are known quantities[22,26]. For 2-methylphenylene group, a similar method has been applied to derive its spectra by comparison with the spectra between mesitylene and 1,2,4,6-methylbenzene, as was used for the spectra derivation of 2,6-dimethylphenylene group[22]. Two new stretching vibrations are related to nitrogen: N=C and N–ϕ. One can find these two stretching modes either from infra-red spectra of the polymers or from small-molecule analogues. They are 2331 K for N=C* and 1822–1957 K for N–ϕ[27]. The value of θ_1 is a linear function of the square root of F_{rigid}, where F_{rigid} is the weight fraction of the rigid mesogenic group in the PAMEs[28]. We thus have:

$$\theta_1 = 760.6 - 192.3 F_{rigid}^{1/2} \quad (4)$$

Based on equation (4) one has $\theta_1 = 598$ and 606 K for PAMEs ($n = 3$ and 4), respectively. Further assumptions were made as to the value of θ_3; according to our experiences, this was taken to be 40 K[22]. In order to convert C_p to C_v, A_0 ranged between 6.00×10^{-3} and 8.50×10^{-3} K mol J^{-1}, which is in a reasonable range for most polymers (6.00×10^{-3} for PAME ($n = 1$), 7.00×10^{-3} for PAME ($n = 2$) and 8.50×10^{-3} for PAMEs ($n = 3$ and 4)). The values of T_m° were selected from modified T_d (574 K for PAME ($n = 1$), 480 K for PAME ($n = 2$), 456 K for PAME ($n = 3$) and 408 K for PAME ($n = 4$))†.

The standard deviation between calculated and experimental data is $\pm 0.3\%$ for PAME ($n = 1$) and $\pm 0.2\%$ for PAME ($n = 2$) in a narrow temperature range. There are no deviations that can be calculated for the other two PAMEs because of insufficient experimental data. Two calculated solid heat capacities for PAMEs ($n = 3$ and 4) can be cast in the following equations:

$$C_p = 0.002\,4868 T^2 + 0.668\,66 T + 170.17 \quad (5)$$

and

$$C_p = 0.003\,2512 T^2 + 0.528\,64 T + 212.38 \quad (6)$$

in J K^{-1} mol^{-1}. The contributions to the solid heat capacities from both skeletal and group vibrations to C_v, as well as the calculated and experimental C_p values for PAME ($n = 1$), as an example, are shown in *Figure 3*.

Heat capacities in mesophase and liquid states

In the temperature range between their glass transition temperatures T_g and isotropic transition temperatures T_i, the heat capacities of the mesophases can be measured for PAMEs ($n = 2$, 3 and 4). For PAME ($n = 1$), one can measure the heat capacity up to its decomposition temperature, since the decomposition temperature is lower than its T_i. Above the isotropic transition temperatures, their isotropic liquid heat capacities can also be detected for PAMEs ($n = 2$, 3 and 4). We have found that the heat capacities in both states can be substantially fitted to one linear relationship, for all PAMEs ($n = 2$, 3 and 4). Assuming that it is also true for PAME ($n = 1$), we thus have:

$$C_p = 0.8419 T + 371.82 \quad \text{for PAME } (n = 1) \quad (7)$$

$$C_p = 0.9086 T + 439.73 \quad \text{for PAME } (n = 2) \quad (8)$$

$$C_p = 0.9751 T + 507.78 \quad \text{for PAME } (n = 3) \quad (9)$$

$$C_p = 1.0417 T + 575.53 \quad \text{for PAME } (n = 4) \quad (10)$$

in J K^{-1} mol^{-1}.

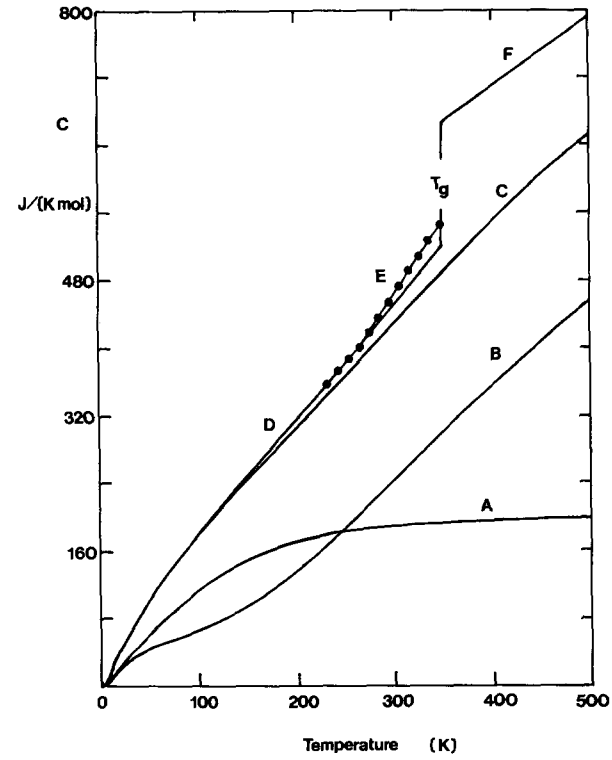

Figure 3 Computed and experimental heat capacities of PAME ($n = 1$). Mesophase glassy solid state: A, skeletal contribution (Tarasov function, $\theta_1 = 580$ K, $\theta_3 = 40$ K, $N_s = 25$); B, group contributions ($N_g = 125$); C, total, computed heat capacity at constant volume; D, computed heat capacity at constant pressure; E, experimental points. Mesophase state: F, experimental data between the glass transition $T_g = 350$ K and 600 K (heat capacity at constant pressure)

* From our *FT*i.r. measurement. The stretching vibrational frequency was observed at 1620 cm^{-1}, which is equivalent to 2331 K (see text)

† Since T_d values of PAMEs (see *Table 2*) observed from experiments are not equilibrium data, we have added 40 K to each observed result as a first approximation in order to approach their equilibrium states, the reason being that one must match the increase of 25.3 J K^{-1} mol^{-1} for the entropy change of poly(ethylene oxide) for the disordered transitions from PAME with $n = i$ to $n = i + 1$ ($i = 1$, 2 and 3) (see the 'Discussion' section in the text)

The standard deviations for 10 runs of each polymer are ±1.2%, ±1.1%, ±1.2% and ±1.0% for the four polymers, respectively.

Glass transitions of mesophase and semicrystalline states

After heating the samples to above their disordering transition temperatures T_d, and quenching ($n=1$) or cooling ($n=2$, 3 and 4) to 230 K, single mesophase glassy states are formed. It is now possible to study the mesophase glass transitions. *Figure 4* reveals the four mesophase glass transition regions. For PAME ($n=1$), the liquid heat capacity is extrapolated from high temperatures (broken line) since the polymer crystallizes as soon as its glass transition region is passed. The chain lines are the calculated solid heat capacities for the four PAMEs. They permit us to study the heat capacity increase at T_g, ΔC_p. The results are listed in *Table 2*, together with the five characteristic temperatures. One can find that for PAMEs ($n=3$ and $n=4$) the beginning glass transition temperature, T_b, is substantially below 230 K, which was our measurement limit. The values of T_b increase with a decrease in the number of flexible spacers (n). The same tendencies can be observed for the other four temperatures, namely, T_1, T_g, T_2 and T_e, as listed in *Table 2* (see also *Figure 8*). The relationship between T_g and the number of flexible spacers is not linear but exponential. Of major interest is that between T_b and T_g; a 70 K temperature range is involved. A pre-glass transition exists for every PAME. Such pre-glass transition regions can be approximately characterized by the temperature range between T_b and T_g. The contribution of ΔC_p to the pre-glass transition increases with the number of flexible spacers (n).

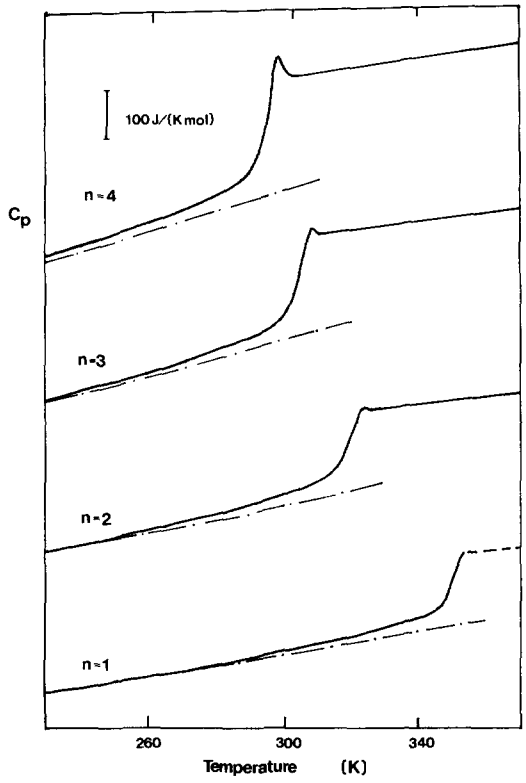

Figure 4 Glass transition temperature regions of PAMEs ($n=1$, 2, 3 and 4). The broken line is the heat capacity extrapolated from high temperature for PAME ($n=1$). The chain lines are the calculated solid heat capacities for the PAMEs

In *Table 2*, data for four semicrystalline samples of the PAMEs, as polymerized, are also listed for comparison with these mesophase glass transitions. Both the broadness of the major glass transition (ΔT_1) and the width of the glass transition (ΔT_2) can be observed in the semicrystalline samples. Only a part of the ΔC_p compared with the data of mesophase glass transitions can be seen, which represents mobile portions in the samples. They are also listed in *Table 2*. The most interesting result is from the semicrystalline sample of PAME ($n=4$), where two glass transition temperatures are observed. The lower T_g is at 298 K, which contributes about 140 J K^{-1} mol^{-1} of the ΔC_p, and the higher T_g is at 325 K, which contributes about 40 J K^{-1} mol^{-1}. This leads to a total heat capacity increase of 180 J K^{-1} mol^{-1} (see *Table 2*). However, such phenomenon of two glass transition temperatures for PAME ($n=4$) does not exist in the mesophase glass transitions (*Figure 4*). Only one glass transition temperature (293 K), contributed by 238 J K^{-1} mol^{-1} of the ΔC_p, is observed over 110 K of the glass transition region.

Hysteresis effect of mesophase glass transitions

Figure 5 represents an example of PAME ($n=4$), showing the hysteresis of the heat capacity on cooled PAMEs in the mesophase glass transition region. Since cold crystallization occurs immediately after the glass transition of PAME ($n=1$), the hysteresis effect cannot be studied. The largest endothermic hysteresis peaks are observed at a cooling rate of 0.31 K min^{-1} for the three PAMEs. The heats of hysteresis peaks are 315.4, 472.5 and 630.7 J mol^{-1} for PAMEs ($n=2$, 3 and 4), respectively. With increasing cooling rate the endotherms

Table 2 Thermal properties of PAMEs in the glass transition region measured on heating at 10 K min^{-1}

PAMEs	T_b (K)	T_1 (K)	T_g (K)	T_2 (K)	T_e (K)	ΔT_1 [a] (K)	ΔT_2 [a] (K)	ΔC_p (J K^{-1} mol^{-1})
$n=1$	270	345	350	354	(362)[b]	9	92	137.3
	270	345	362	374	384	29	114	55
$n=2$	240	313	318	323	330	10	90	173.9
	240	313	331	341	350	28	110	118
$n=3$	(220)[b]	300	305	310	317	10	97	199.7
	(220)	300	320	332	340	26	120	112
$n=4$	(195)[b]	288	293	297	305	9	110	234.4
	(195)	288, 319	298, 325	307, 330	315, 335	15, 11	120, ?[c]	180

[a] ΔT_1 and ΔT_2 are defined as T_2-T_1 and T_e-T_b, respectively
[b] Temperatures in parentheses are extrapolated data (see text for details)
[c] The semicrystalline sample of PAME ($n=4$) shows two glass transitions, and the second value of ΔT_2 for that sample cannot be determined (?)

decrease as shown in *Figure 5*. The relationship between Δh and logarithmic cooling rate is shown in *Figure 6*. The data deviate from a straight line above a cooling rate of 1.25 K min^{-1}, similar to the case of poly(oxy-2,6-dimethyl-1,4-phenylene) (PPO)[29] and poly(ethylene 2,6-naphthalene dicarboxylate) (PEN)[30]. With an increase in the number of flexible spacers (n), one can find that the hysteresis effect becomes increasingly larger. Quantitatively, such an increase follows a rule of (constant × n) at fixed cooling rate. Finally, no hysteresis peak is observed in the semicrystalline PAME samples.

First-order transitions of PAMEs

The transitions from crystalline to mesophase states and to isotropic melts for the PAMEs show first-order transitions, based on our d.s.c. measurements. Their transition temperatures (T_d and T_i values) are listed in *Table 1*. *Figure 7* shows two d.s.c. heating curves for PAME ($n=3$), as an example. Curve A is semicrystalline PAME ($n=3$) as polymerized, and curve B, by comparison, is totally mesophase PAME ($n=3$). With an increasing number of flexible spacers (n), one can find that both T_d and T_i values of PAMEs decrease, as shown in *Figure 8*. The enthalpy changes of disordered transitions of the PAMEs measured here are from semicrystalline

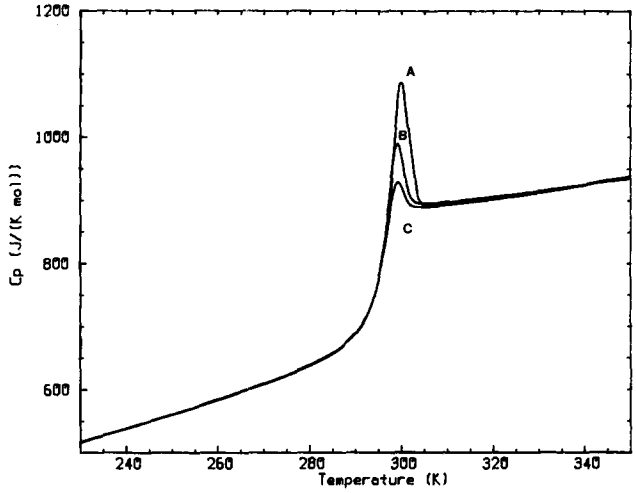

Figure 5 Hysteresis in heat capacity of mesophase PAME ($n=4$) in the glass transition region at different cooling rates: (A) 0.31 K min^{-1}; (B) 2.5 K min^{-1}; and (C) 10 K min^{-1} before heating at 10 K min^{-1}

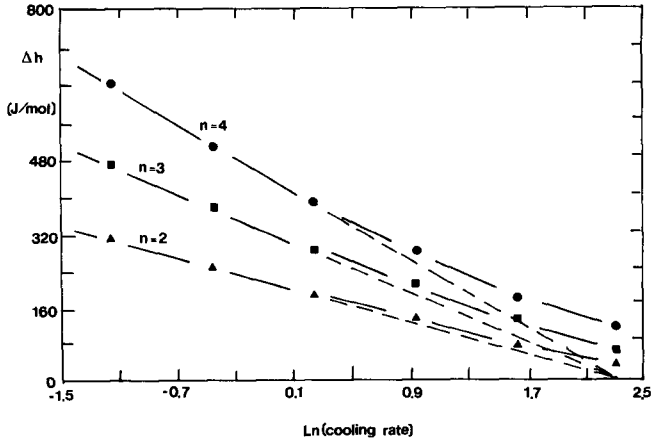

Figure 6 Relationship between the enthalpy under the hysteresis peak and the logarithm of the cooling rate for mesophase PAMEs ($n=2$, 3 and 4). Heating rate is 10 K min^{-1} (ln 10 = 2.303)

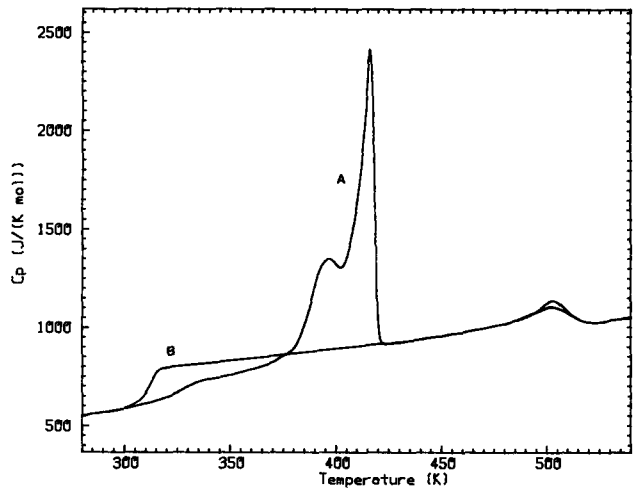

Figure 7 D.s.c. heat traces of PAME ($n=3$): (A) as polymerized semicrystalline sample; (B) sample cooled from the isotropic melt to 220 K and measured at a heating rate of 10 K min^{-1}

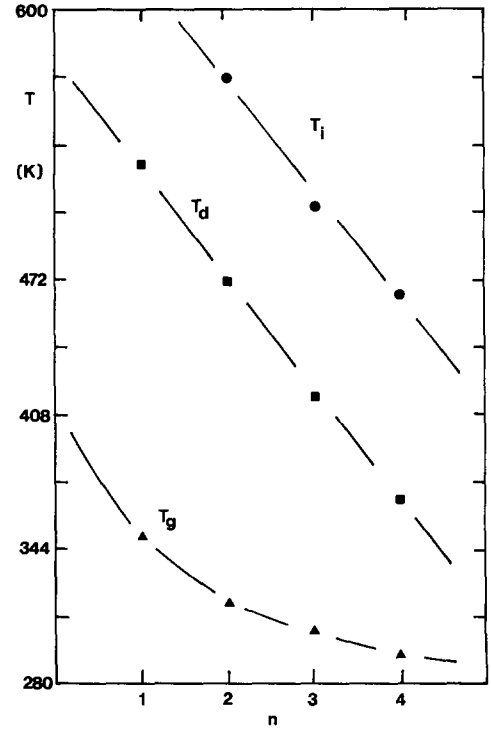

Figure 8 Relationship between the glass transition temperature T_g, disordered transition temperature T_d, isotropic transition temperature T_i, and the number of flexible spacers n

samples. Based on our X-ray data, their crystallinities can be determined and are listed in *Table 1*. Therefore, the enthalpies of the transitions of 100% crystallinities can be calculated, and are also listed in *Table 1*. One can see that the enthalpy changes of the semicrystalline samples in the transitions are strongly correlated with the odd or even number of flexible spacers.

However, the equilibrium enthalpies increase with the number of flexible spacers with an almost constant value of 8 kJ mol^{-1} for each additional unit of ethylene glycol. The entropy changes of the disordering transitions, as listed in *Table 1*, have the same tendency. The differences of entropy change between $n=1$ and 2, as well as $n=3$ and 4, are larger, 34.3 and 38.9 J K^{-1} mol^{-1}, respectively, compared with that between $n=2$ and 3, of 25.8 J K^{-1} mol^{-1}. For the enthalpy changes of isotropic transitions (T_i values), one can also find that it increases

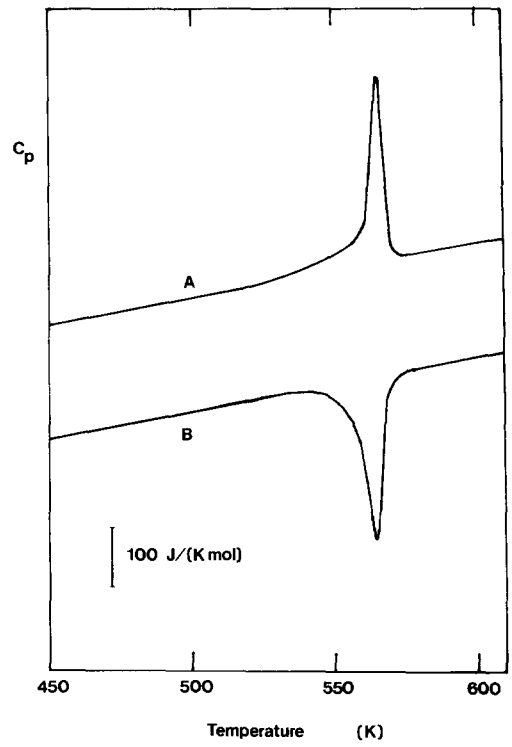

Figure 9 D.s.c. heating (A) and cooling (B) traces in the isotropic transition temperature region for PAME ($n=2$). Both heating and cooling rates are 10 K min^{-1}

with the number of flexible spacers, as shown in *Table 1*. An increase of 0.7 J K^{-1} mol^{-1} for the addition of each extra ethylene glycol is observed. Furthermore, the transitions studied here did not indicate large supercooling when the samples were cooled from their isotropic melts, as shown in *Figure 9* for PAME ($n=2$), as an example.

DISCUSSION

Nematic liquid-crystalline PAMEs

The three main supporting pieces of evidence reported have convinced us that, for the PAMEs studied, there is a nematic liquid-crystalline phase before they reach their isotropic melts: namely, the patterns of flowed schlieren textures observed in polarized optical microscopy; the X-ray diffraction pattern in the mesophase states; and the entropy changes of the isotropic transitions (T_i). It is well known that the flowed schlieren texture with thread-like lines is a typical optical characterization of a nematic liquid-crystalline phase[31]. Information concerning this texture has been studied by Friedel[32] and others in detail. The results from X-ray diffraction in the nematic phase have shown that from *Figure 2* there is a strong diffuse ring at an angle of $2\theta=21.4°$, which is a measure of the distance between neighbouring chain molecules with an average value of about 0.42 nm. The large width of the reflections indicates quite clearly that only a short-range positional order exists in the nematic phases[33]. The d.s.c. measurements have indicated that there is a low entropy change during the transitions from nematic phases to isotropic melts of the PAMEs studied here (*Table 1*). It seems to be a common observation in all liquid-crystalline polymers, especially for nematic liquid-crystalline polymers[15], revealing that the orientational order in the nematic liquid crystals is quite imperfect.

Heat capacities of PAMEs

The calculations of solid heat capacities of PAMEs have provided another set of successful examples to prove the utility of this method. In our case, not only the calculations but also the predictions of solid heat capacities of PAMEs ($n=3$ and 4) have been carried out, based on an addition scheme which has shown that the heat capacities of similar macromolecules may be predicted from this scheme by adding group vibrations and trends in θ_1 (equation (4)) and θ_3 (unchanged). One can find that the solid heat capacities of PAMEs ($n=1, 2$, 3 and 4) differ only in the contribution of one ethylene glycol in each case. The heat capacities in nematic phases can be substantially fitted to the linear relationships of heat capacities with respect to temperature in their own isotropic melts. A similar observation has been reported for thermotropic copolyesters[34], indicating that for the anisotropic molten state the heat capacity is most likely similar to that of the isotropic state. It can also be understood by the fact that the specific volume in liquid crystals is close to that of the isotropic melt[35]. It is thus a natural extension that the heat capacities of PAME ($n=1$) can be recognized as the same as its liquid heat capacities in the isotropic melt. The four liquid heat capacities described in equations (7) to (10) show linear relationships with temperature. Yet, the reason for such a linear relationship is quantitatively not well understood. Qualitatively, an exponential increase of the heat capacity due to the contributions from group vibrations with temperature in our experimental range is compensated by two negative contributions caused by a displacement of backbone motion from a torsional oscillation to a rotation during the transitions, and by the two-state contribution of the hole–no-hole equilibrium to the heat capacity. A quantitative proof of this explanation has been tested for polymers with relatively simple chemical structures on the basis of detailed pvT data and statistical mechanics[36].

The best approach to liquid heat capacities of macromolecules is presently still an empirical addition scheme[37]. The heat capacities of the present four PAMEs (equations (7) to (10)) have shown that, indeed, the difference in the liquid heat capacities between PAMEs with $n=i$ and $n=i+1$ ($i=1, 2$ and 3) correlates well with the liquid heat capacities for poly(ethylene oxide) (PEO), which is formulated to be[38]:

$$C_p=0.668T+67.85 \qquad (11)$$

in J K^{-1} mol^{-1}.

Glass transition regions

After the determination of the heat capacities in both solid and liquid/LC states, it is now possible to find the heat capacity increase at the glass transition temperatures for the PAMEs. First, the correlations between glass transition temperature T_g and the number n of flexible spacers are not linear, but rather exponential. A similar observation can be obtained for the other four characterized temperatures around the glass transition region. This behaviour must therefore be related to a structural relaxation process which increases exponentially with n. The pre-glass transition regions observed here, secondly, are mainly contributed by the flexible spacer. Note that the glass transition of PEO is in the region of 206 K with a heat capacity increase[38] of

35.2 J K^{-1} mol^{-1} at T_g. It can be further indicated by an increase of ΔC_p at the pre-glass transition with n. The wide temperature range (over 70 K) for the pre-glass transition is most likely caused by the connection between flexible spacer and rigid mesogenic group.

If a hindering effect is caused by the existence of the crystals, then two separate glass transitions are possible, which may be attributed to two different amorphous portions, namely, normal and rigid amorphous portions[19,29,30], as shown in the semicrystalline PAME ($n=4$) (*Table 2*). Therefore, one can still distinguish the two different contributing portions for ΔC_p in the cases of the PAMEs even though one glass transition is only apparent in most liquid-crystalline polymers. A more detailed and precise determination of the solid heat capacities of the polymer studied is, therefore, perhaps necessary. Thirdly, it is surprising that the hysteresis effect is a function of the number of flexible spacers. The more rigid the chain is (smaller n), the lower the heat of the hysteresis peak will be. In principle, the hysteresis effect is a characterization of the kinetics of structural relaxation. Our results indicate that such structural relaxation relies on the chain flexibility. On the other hand, the positive deviations from the linear relationship in *Figure 6* indicate that the freezing and unfreezing of molecular motion in the PAME samples at the glass transition temperature is asymmetric. A similar situation has been observed in the case of PPO[29] and PEN[30]. The PAMEs studied here yield yet another set of examples to fit our previous expectation for such positive deviation in hysteresis study, namely, polymer chains with a backbone width larger than that of a phenylene group (0.5 nm) would appear to be the cause of such positive deviation (see the chemical structures of PAMEs).

Semicrystalline PAME samples, in most cases, show no hysteresis. The broadening of the glass transition region (*Table 2*) is not sufficient to explain the disappearance of hysteresis. The interaction between crystal and mesophase must then reduce the time dependence of the glass transition, as was recently found for other semicrystalline polymers, such as poly(ethylene terephthalate)[39].

For the semicrystalline PAMEs as polymerized, their glass transition regions are broadened due to the existence of the crystalline phase by the displacement of glass transition temperature T_g, extrapolated ending temperature T_2, and the ending glass transition temperature T_e. The beginning and extrapolated beginning glass transition temperatures, T_b and T_1, however, remain unchanged (*Table 2*).

Finally, it is surprising to observe how well the estimation of the heat capacity increase at T_g for the PAMEs works, based on the suggestion of a constant (11.3 J K^{-1} mol^{-1}) contribution to ΔC_p per mobile bead[40]. Even though dividing the bead is still somewhat ambiguous theoretically, we can predict, as a first approximation based on our experience, values of 135.6, 169.5, 203.4 and 237.3 J K^{-1} mol^{-1} for the PAMEs ($n=1$, 2, 3 and 4), respectively*. Our heat capacity increases at T_g, ΔC_p, listed in *Table 2*, are indeed very close to the data estimated here.

*Based on the chemical structures of PAMEs, the groups CH_2–, O–, N=CH– are referred to as 'small' beads. Their ΔC_p is 11.3 J K^{-1} mol^{-1}. The groups C_6H_4–, C_7H_6– are referred to as 'large' beads. Their ΔC_p is double that of a small bead

Transition enthalpies and entropies

From *Figure 8*, linear relationships between disordered transition temperature T_d, isotropic transition temperature T_i, and the number of flexible spacers have been observed with very close slopes. Unfortunately, since we have introduced an oxygen atom into the flexible spacer, the odd–even effect with increasing flexible spacer length may occur, but intermediate lengths of such spacers were not available. Therefore, it is difficult to draw any specific conclusions on this effect. However, an interesting fact is that the PAMEs with an even number of flexible spacers show relatively low degrees of crystallinity (26.9% for $n=2$ and 19.1% for $n=4$) compared with the PAMEs with an odd number of flexible spacers (almost double, see *Table 1*). From our X-ray diffraction experiments, in fact, we have found there there are two different crystalline structures present in the PAMEs of even and odd numbers of flexible spacers, and they will be discussed in detail in the second paper of this series[21]. Based on the crystallinities determined by both X-ray and d.s.c. measurements, the enthalpy changes of disordered transitions of 100% crystallinities can be estimated. Interestingly, one can see that the difference of the enthalpy changes between two neighbouring n is about 8 kJ mol^{-1}. Again, it is worth while to note that the enthalpy change of low-molecular-mass PEO is 7.9 kJ mol^{-1} (ref. 41). On the other hand, our results of the semicrystalline PAMEs indicate that, at least for the even numbers $n=2$ and $n=4$, the flexible spacer (ethylene glycol) does not contribute to the crystalline states of PAMEs. It is well known that PEO has a conformation of 3*7/2 in the crystalline state[42]. Obviously, even $n=4$ cannot completely form a crystalline repeat unit. Nevertheless, different linkages for different n may significantly influence the crystalline structure[21].

Based on the thermodynamic relation $\Delta S=\Delta H/T$, one can calculate the entropy changes of the transitions. It has been found that the entropy change increases with the number of flexible spacers from 75.5 J K^{-1} mol^{-1} for $n=1$ to 174.5 J K^{-1} mol^{-1} for $n=4$. An approximation of the contribution for the entropy change during the transition by introducing an extra ethylene glycol is experimentally observed to be 34.3, 25.8 and 38.9 J K^{-1} mol^{-1} for PAMEs ($n=2$, 3 and 4), respectively. These values are somewhat larger than the entropy contribution of PEO during its fusion at 25.3 J K^{-1} mol^{-1} (ref. 43). Such deviations are possibly caused by the non-equilibrium values of the transition temperatures, T_d. Furthermore, one can also recognize that the entropy change from an odd to an even number of flexible spacers is about 10 J K^{-1} mol^{-1} larger than that from an even to an odd number. Such a difference indicates that the metastability of the PAMEs ($n=2$ and 4) are lower than that of the PAMEs ($n=1$ and 3).

Turning to the isotropic transitions of the PAMEs, they are in thermodynamic equilibrium (no supercooling can be observed during cooling, see *Figure 9*). First, the entropy change of the transitions (ΔS_d) indicates that most of the chain order has been lost during the disordered transitions. The observations in polarized optical microscopy (*Figures 1a* and *1b*) indicate, however, that the birefringence still exists in the nematic liquid-crystalline state, revealing a large degree of orientational order. Usually, one describes such an order remaining in the nematic melt by use of the nematic order parameter S. This parameter can be determined by using the

distribution of the intensity of the amorphous halo at constant scattering angle as a function of the azimuthal angle[44]. The value of S is often above 0.80.

We have recognized that, in actual fact, two kinds of measurements provide the order information in different scales. The optical study shows macroscopically a multiple chain orientation among macromolecules. The entropy change of the isotropic transition basically points out microscopically the difference of realizable conformations between two phases. A natural deduction is that, therefore, in a nematic liquid-crystalline polymer orientation among the chains is still retained. However, the realizable conformations within a chain are very close to the isotropic melt. Only chain orientational direction remains. Our observation of the entropy change of the isotropic transition reveals that, even though ΔS_i increases with the number of flexible spacers, as expected, a $0.7\,J\,K^{-1}\,mol^{-1}$ increase is far from a true compensation of adding an extra unit of ethylene glycol.

CONCLUSIONS

A new series of PAMEs has been thermally characterized. One can draw several conclusions:

Nematic liquid-crystalline phases are observed after the disordered transitions of PAMEs. They can form a single LC glassy phase by quenching ($n=1$) and cooling ($n=2$, 3 and 4) to below their LC glass transition temperatures.

The heat capacities of solid states have been measured for $n=1$ and 2, and calculated for $n=1$, 2, 3 and 4, based on infra-red and Raman vibrational spectra as well as dispersion curves. Heat capacities of the liquid-crystalline state have been found to be substantially fitted to those of their own isotropic melts. They show linear relationships with respect to temperature.

The LC glass transition regions of PAMEs have been described. A pre-glass transition has been observed which is mainly attributed to the flexible spacer. Hysteresis studies indicate that in the LC glasses such an effect is dependent upon chain rigidity. A broadening and shifting to high temperatures of the glass transition regions have been observed for the semicrystalline PAMEs.

Equilibrium enthalpy changes for the disordered transitions of PAMEs have been calculated. It increases about $8\,kJ\,mol^{-1}$ by adding an extra flexible spacer. The crystallinities of the semicrystalline samples have been determined by X-ray diffraction measurements. Two different groups of crystallinity based on even or odd numbers of flexible spacers have been observed for the PAMEs. X-ray diffraction patterns reveal that there are two different crystal structures for these two groups.

The isotropic transitions of PAMEs have shown a low enthalpy change, even though the value of ΔS_i increases with the number of flexible spacers. It indicates that a very imperfect nematic liquid-crystalline state exists. The explanation for the difference between small ΔS_i and high order parameter observed in optical microscopy has been attempted.

ACKNOWLEDGEMENT

This work has been supported by the Research Challenge grant of the Ohio Board of Regents through The University of Akron.

REFERENCES

1 Adams, R., Bullock, R. E. and Wilson, W. C. *J. Am. Chem. Soc.* 1923, **45**, 521
2 Marvel, C. S. and Hill, H. W. *J. Am. Chem. Soc.* 1950, **72**, 4819
3 Marvel, C. S. and Tarkoy, N. *J. Am. Chem. Soc.* 1958, **80**, 832
4 Marvel, C. S. and Bonsignore, P. V. *J. Am. Chem. Soc.* 1959, **81**, 2668
5 Cotter, R. J. and Matzner, M. *Org. Chem. (NY)* 1972, **133**(1), 1, 30
6 D'Alelio, G. F. *Encycl. Polym. Sci. Technol.* 1969, **10**, 659
7 Morgan, P. W., Pletcher, T. C. and Kwolek, S. L. *Polym. Prepr., Am. Chem. Soc., Div. Polym. Chem.* 1983, **24**(2), 470
8 Morgan, P. W., Kwolek, S. L. and Pletcher, T. C. *Macromolecules* 1987, **20**, 729
9 Morgan, P. W., US Patents 4048148, 1977 and 4122070, 1978; Fr. Patent 2310426, 1976
10 Milland, B., Thierry, A. and Skoulios, A. *Mol. Cryst. Liq. Cryst. Lett.* 1978, **41**, 263
11 Milland, B. and Strazielle, C. *Polymer* 1979, **20**, 563
12 Milland, B., Strazielle, C. and Weill, G. *Polymer* 1980, **21**, 639
13 Wojtkowski, P. W. *Macromolecules* 1987, **20**, 740
14 Sridhar, K. and Harris, F. W. *Polym. Prepr., Am. Chem. Soc., Div. Polym. Chem.* 1988, **29**(2), 304
15 Wunderlich, B. and Grebowicz, J. *Adv. Polym. Sci.* 1984, **60/61**, 1
16 Harris, F. W. and Sridhar, K. *Polym. Prepr. Am. Chem. Soc., Div. Polym. Chem.* 1988, **29**(2), 308
17 Wunderlich, B. and Bopp, R. C. *J. Thermal Anal.* 1974, **6**, 335; see also Mehta, A., Bopp, R. C., Gaur, V. and Wunderlich, B. *J. Thermal Anal.* 1978, **13**, 197
18 Ginnings, D. C. and Furukawa, G. T. *J. Am. Chem. Soc.* 1953, **75**, 522
19 Cheng, S. Z. D., Cao, M.-Y. and Wunderlich, B. *Macromolecules* 1986, **19**, 1868
20 Sullivan, P. and Wunderlich, B. *SPE Trans.* 1964, **4**, 113
21 Cheng, S. Z. D., Janimak, J. J., Zhang, A. Q., Sridhar, K. and Harris, F. W. in preparation
22 Cheng, S. Z. D., Lim, S., Judovits, L. H. and Wunderlich, B. *Polymer* 1987, **28**, 10; and a series of papers published in *Polymer* during 1985 to 1988 from ATHAS Laboratory
23 Gaur, U., Lau, S.-F., Wunderlich, B. B. and Wunderlich, B. *J. Phys. Chem. Ref. Data* 1981, **10**, 1001
24 Gaur, U., Lau, S.-F. and Wunderlich, B. *J. Phys. Chem. Ref. Data* 1983, **12**, 65, 91
25 Cheban, Yu., Lau, S.-F. and Wunderlich, B. *Colloid Polym. Sci.* 1982, **260**, 9
26 Grebowicz, J., Suzuki, H. and Wunderlich, B. *Polymer* 1985, **26**, 561
27 Silverstein, R. M., Bassler, G. L. and Morrill, T. C. 'Spectrometric Identification of Organic Compounds', 4th Edn., Wiley, New York, 1981
28 Bu, H. S., Cheng, S. Z. D. and Wunderlich, B. *J. Phys. Chem.* 1987, **91**, 4179
29 Cheng, S. Z. D. and Wunderlich, B. *Macromolecules* 1987, **20**, 1630
30 Cheng, S. Z. D. and Wunderlich, B. *Macromolecules* 1988, **21**, 789
31 Hartshorne, N. H. in 'Liquid Crystals and Plastic Crystals' (Eds. G. W. Gray and P. A. Winsor), Halsted, New York, 1974, Vol. 2, Ch. 2
32 Friedel, G. *Ann. Phys.* 1922, **18**, 273
33 de Vries, A. *Mol. Cryst. Liq. Cryst.* 1970, **10**, 219; see also, Wendorff, J. H. in 'Liquid Crystalline Order in Polymers' (Ed. A. Blumstein), Academic Press, New York, 1978, Ch. 1
34 Cheng, S. Z. D., Pan, R., Bu, H. S. and Wunderlich, B. *Makromol. Chem.* 1988, **189**, 1579
35 Smith, G. W. in 'Advances in Liquid Crystals', Vol. 1, 'Plastic Crystals, Liquid Crystals, and the Melting Phenomenon. The Importance of Order' (Ed. G. C. Brown), Academic Press, New York, 1975
36 Loufakis, K. and Wunderlich, B. *J. Phys. Chem.* 1988, **92**, 4205
37 Pan, R., PhD Thesis, Department of Chemistry, Rensselaer Polytechnic Institute, Troy, NY, 1988
38 Suzuki, H. and Wunderlich, B. *J. Polym. Sci., Polym. Phys. Edn.* 1985, **23**, 1671
39 Menczel, J. and Wunderlich, B. *J. Polym. Sci., Polym. Lett. Edn.* 1981, **19**, 261
40 Wunderlich, B. *J. Phys. Chem.* 1960, **64**, 1052
41 Cheng, S. Z. D. and Wunderlich, B. *J. Polym. Sci., Polym. Phys. Edn.* 1986, **24**, 577
42 Tadokoro, H. *J. Polym. Sci. (C)* 1966, **15**, 1
43 Wunderlich, B. 'Macromolecular Physics', Vol. 3, 'Crystal Melting', Academic Press, New York, 1980
44 de Gennes, P. G. 'The Physics of Liquid Crystals', Clarendon, Oxford, 1974; see also Leadbetter, A. and Norris, E. K. *Mol. Phys.* 1979, **38**, 669